Contrib Mineral Petrol (2007) 153:465–481
DOI 10.1007/s00410-006-0160-x

ORIGINAL PAPER

Cryptic crustal contamination of MORB primitive melts recorded in olivine-hosted glass and mineral inclusions

Vadim S. Kamenetsky · Andrey A. Gurenko

Received: 13 July 2006 / Accepted: 6 November 2006 / Published online: 5 December 2006

Abstract The origin of compositional heterogeneities among the magmas parental to mid-ocean ridge basalts (MORB) was investigated using a single rock piece of the olivine-phyric basalt from 43°N, Mid-Atlantic Ridge (AII D11-177). The exceptional feature of this sample is presence of very primitive olivine crystals (90–91 mol% Fo) that are significantly variable in terms of CaO (0.15–0.35 wt%). A population of low-Ca olivine (0.15–0.25 wt% CaO) is also notably distinct from high-Ca olivine population in AII D11-177, and primitive MORB olivine in general, in having unusual assemblage of trapped mineral and glass inclusions. Mineral inclusions are represented by high-magnesian (Mg# 90.7–91.1 mol%) orthopyroxene and Cr-spinel, distinctly enriched in TiO_2 (up to 5 wt%, c.f. <1 wt% in common MORB spinel). Glass inclusions associated with orthopyroxene and high-Ti Cr-spinel have andesitic compositions (53–58 wt% SiO_2). Compared to the pillow-rim glass and "normal" MORB inclusions, the Si-rich glass inclusions in low-Ca olivine have strongly reduced Ca and elevated concentrations of Ti, Na, K, P, Cl, and highly incompatible trace elements. Strong variability is recorded among glass inclusions within a single olivine phenocrysts. We argue that the observed compositional anomalies are mineralogically controlled, and thus may arise from the interaction between hot MORB magmas and crystal cumulates in the oceanic crust or magma chamber.

Keywords MORB · Melt inclusions · Olivine · Orthopyroxene · Spinel · Felsic magmas · Mantle · Oceanic crust · Assimilation

Introduction

The last two decades of petrological and geochemical studies on mid-ocean ridge basalts (MORB), their cumulative counterparts in the oceanic crust and their ancient analogs in ophiolites have seen rapidly accumulating evidence for heterogeneous compositions of MORB parental melts. Recent advances in melt inclusion studies defined new compositional types of MORB parental melts (e.g., ultra-depleted, ultra-enriched, ultra-calcic) in addition to widespread depleted (normal) and enriched MORB (e.g., Danyushevsky et al. 1987; Sobolev and Shimizu 1993a, b; Sobolev 1996; Kamenetsky et al. 1998, 2000). Recorded variability in major and trace elements and isotopic compositions is most commonly attributed to chemical and phase inhomogeneities in the mantle source peridotite, juxtaposition of several mantle sources (including plume- and subduction-related), varying physical parameters of melting, and melt-peridotite reactions (see reviews in Langmuir et al. 1992; Hofmann 2003). However, the origin of compositional complexity and anomalous compositions among MORB solely due deep-seated processes is often challenged by research on oceanic cumulates (Bédard 1991, 1993; Ross and

---

Communicated by Jochen Hoefs.

V. S. Kamenetsky (✉)
ARC Centre of Excellence in Ore Deposits,
School of Earth Sciences, University of Tasmania,
Hobart 7001, Australia
e-mail: Dima.Kamenetsky@utas.edu.au

V. S. Kamenetsky · A. A. Gurenko
Max-Planck-Institut für Chemie, Abteilung Geochemie,
Postfach 3060, 55020 Mainz, Germany

Elthon 1993; Amri et al. 1996; Bédard and Hébert 1996; Bédard et al. 2000; Gillis et al. 2003; Koepke et al. 2005b; Nonnotte et al. 2005). ‘‘If reactions between primitive basaltic melts and shallow peridotitic mantle are plausible, then such melts should also react strongly with lower-crustal rocks...Oddly enough, the possible importance of reactions between ascending primitive melts and crustal rocks in oceanic environment has received little attention’’ (Bédard et al. 2000). Supportive of this view and alternative to conventional wisdom, the concept of localised processes of dissolution, reaction and mixing (DRM) in the magmatic plumbing system was applied in interpretation of some anomalous compositions of melt inclusions in primitive MORB phenocrysts (Danyushevsky et al. 2003, 2004).

The interaction between ‘‘normal’’ MORB primitive melts and refractory mantle peridotite has been proposed to account for unusual assemblage of high-Si, low-Ca melt inclusions, high-Ti Cr-spinel and orthopyroxene in forsteritic olivine from the sample AII32 D11-177, 43°N Mid-Atlantic Ridge (Kamenetsky and Crawford 1998). In present study this sample is revisited with application of improved high-precision electron microprobe and laser ablation ICP-MS analyses of major and trace elements in minerals and melt inclusions, and the earlier constraints are revised in the light of new results. In this case modifications of MORB primitive melts caused by interaction with crustal gabbroic rocks appear to be most plausible explanation for anomalous mineral and melt inclusion compositions.

Samples

The studied sample was recovered from dredge 11 of the 32nd cruise of the R/V Atlantis II. The dredge sampled the eastern slope of the Mid-Atlantic Ridge rift valley 42°57′N 29°15′W at 1,983–2,168 m water depth (Phillips et al. 1969; Shibata et al. 1979). The ridge segment is adjacent to the 43°N fracture zone, which is characterised by exceptionally refractory abyssal peridotites (Shibata and Thompson 1986). Basaltic rocks in this area are compositionally diverse, and in general display enrichment in incompatible trace elements (Shibata et al. 1979). The sample D11-177 is represented in our study by one small rock piece (~3 × 2 × 2 cm) of olivine-phyric basalt with devitrified glassy interior and quenched glass surface. The glass is characterised by relatively primitive composition (Table 1) with high Mg# ($100 \times \mathrm{Mg}/(\mathrm{Mg} + \mathrm{Fe}^{2+}) = 68.8$) and 140 ppm Ni, and unradiogenic Nd and radiogenic Sr and Pb isotope ratios (^{143}Nd/^{144}Nd 0.512924, ^{87}Sr/^{86}Sr 0.703293, ^{206}Pb/^{204}Pb 19.577, ^{207}Pb/^{204}Pb 15.594, and ^{208}Pb/^{204}Pb 39.176), typical of the magmas in this region (Ito et al. 1987; Yu et al. 1997; Kamenetsky et al. 1998).

Olivine phenocrysts (~ 10–15 vol%, up to 4 mm in size) contain euhedral inclusions of reddish-brown and greenish-brown spinel (up to 50 μm), inclusions of light-brown glass of variable shape (round to negative-crystal shaped with scalloped edges) and size (up to 150 μm), vapour bubbles and sulphide globules. There is no particular pattern in the distribution of large melt inclusions; however, smaller inclusions of glass, vapour and sulphide often coexist in subparallel and orthogonal trails (Fig. 1). Individual crystals of reddish-brown spinel are also present in matrix glass.

Analytical techniques

Electron microprobe

Major elements in minerals and glasses and element mapping were performed using the JEOL Superprobe JXA-8200 electron microprobe (Max Planck Institute for Chemistry, Mainz, Germany). We applied 15 kV accelerating voltage, 12 nA electron beam current and defocused to 5 μm size beam for analyses of host matrix glasses and olivine-hosted glass inclusions. The 20 kV and 20 nA primary beam was applied for analyses of olivine and spinel. Peak counting times on major elements were 60 and 30 s of background. Either PRZ or ZAF correction routines were used. Sulphur was analysed at the same analytical conditions as other major elements in glasses. At these conditions, the detection limit for S was around 200–250 ppm. A set of reference materials (i.e. natural and synthetic oxides, minerals and glasses; Micro-Analysis Consultants Ltd, Cambridgeshire, UK and the Smithsonian Institution standard set for electron microprobe analysis, Jarosewich et al. 1980) were used for routine calibration and instrument stability monitoring. Typical analytical uncertainties (2RSD = 2σ relative standard deviation) are 1.4–2.8% for SiO_2, Al_2O_3, FeO, MgO, CaO, TiO_2; 5.6% for Na_2O, 10.1% for K_2O, 15.8% for P_2O_5, and 32.2% for MnO. As a monitor sample to control precision and accuracy of S and Cl measurements, we used the USNM 111240/52 VG-2 basaltic glass (recommended values of 0.134–0.137 wt% S, Dixon et al. 1991; Thordarson et al. 1996; 0.030 wt% Cl, Métrich et al. 2001). The concentrations of 0.140 ± 0.023 wt% S and 0.029 ± 0.007 wt% Cl (±2σ SD = 2-sigma standard deviation, $N = 37$) were obtained during this study.

Table 1 Representative major (in wt%) and trace (in ppm) element compositions of olivine-hosted glass inclusions and pillow-rim glass

N	1	2	3	4	5	6	7	8	9	10	11	12	13	14	15	16	17
Grain	D11-177	m284-30/1	m284-17/1	m284-5/1	m284-38/1	m465a-7/1	m465a-7/2	m465a-17/1	m465a-18/1	m465a-18/2	m465b-5/3	m465a-2/1	m284-32/1	m284-40/1	m465b-7/1	m465b-7/2	m465b-6/1
SiO_2	50.12	49.85	49.60	50.17	50.50	51.26	51.65	50.73	50.09	55.03	57.39	57.76	53.09	56.48	56.87	48.57	54.24
TiO_2	0.95	1.01	1.10	0.99	1.04	1.64	1.40	0.89	0.99	1.34	3.18	2.61	1.63	1.29	2.79	4.88	2.64
Al_2O_3	15.32	16.17	15.27	14.55	15.35	17.45	17.51	16.66	15.40	16.65	15.91	15.75	16.90	15.18	15.23	13.43	14.38
FeO	7.78	7.24	7.63	8.05	6.93	6.38	6.20	6.74	7.47	5.55	5.41	5.17	6.14	5.60	5.96	7.41	6.64
MnO	0.13	0.14	0.16	0.15	0.12	0.12	0.17	0.14	0.16	0.12	0.12	0.13	0.13	0.09	0.15	0.18	0.11
MgO	8.67	8.27	8.66	8.87	8.22	3.88	3.74	6.85	7.85	4.42	3.60	3.43	6.08	6.73	4.84	5.11	5.73
CaO	13.32	13.52	13.97	13.99	14.65	14.33	14.29	12.70	13.42	11.12	8.81	9.74	10.86	9.44	9.38	12.22	11.16
Na_2O	2.19	1.95	1.95	1.96	1.78	2.03	2.03	1.99	2.22	3.29	2.95	2.93	3.49	3.50	2.94	1.90	2.32
K_2O	0.25	0.59	0.45	0.34	0.14	1.64	1.74	1.40	0.28	1.41	1.93	1.50	0.98	0.72	0.71	0.25	0.60
P_2O5	0.11	0.32	0.16	0.12	0.03	0.19	0.21	0.18	0.10	0.02	0.06	0.02	0.10	0.32	0.18	4.55	1.22
Cl	0.02	0.05	0.04	0.03	0.02	0.18	0.20	0.15	0.02	0.10	0.13	0.13	0.07	0.06	0.06	0.13	0.06
S	0.08	0.08	0.09	0.10	0.02	0.02	0.02	0.05	0.04	0.03	0.06	0.01	0.01	0.05	0.06	0.06	0.07
Total	98.94	99.19	99.08	99.32	98.80	99.12	99.16	98.48	98.04	99.08	99.55	99.18	99.48	99.46	99.17	98.69	99.17
CaO/Al_2O_3	0.87	0.84	0.91	0.96	0.95	0.82	0.82	0.76	0.87	0.67	0.55	0.62	0.64	0.62	0.62	0.91	0.78
Fo_Ol		90.9	90.6	90.4	90.5	91.0	90.9	90.9	90.6	90.6	90.1	90.2	90.3	90.3	90.3	90.2	90.3
CaO_Ol		0.28	0.32	0.34	0.32	0.31	0.30	0.29	0.30	0.25	0.16	0.22	0.23	0.19	0.16	0.15	0.18
Sc	40.5	40.7	42.4	45.5	42.8	43.7	46.2	36.4	40.8	39.8	38.8	34.5	36.1	34.9	39.4	51.5	41.2
Rb	5.81	21.4	9.59	8.05	2.22	85.9	92.8	62.1	6.3	41.9	57.9	33.5	27.5	19.4	22.0	2.13	17.8
Sr	157	141	218	191	411	77.7	65.2	69.3	172	401	510	235	302	435	303	1310	578
Y	16.7	17.4	14.3	15.2	16.4	18.3	17.1	16.4	17.5	12.7	16.8	14.9	14.9	12.4	16.5	31.0	18.2
Zr	51.2	89.6	62.8	50.9	41.2	142	155	76.6	53.9	203	229	299	143	171	226	368	270
Nb	9.3	31.0	16.1	12.2	4.3	88.1	99.3	40.3	10.4	9.4	19.6	22.7	9.6	31.3	18.22	152	47.4
Ba	70.3	111.7	114.3	92.6	59.3	201	225	189	79.5	334	591	348	292	233	227	179	232
La	6.83	9.15	11.1	8.6	5.86	11.3	14.1	10.9	7.93	3.77	11.6	16.8	6.6	20.9	6.70	130	61.9
Ce	15.26	21.3	23.1	18.4	13.9	17.6	20.0	20.6	17.0	6.91	25.2	27.0	11.1	44.8	17.9	308	134
Nd	8.81	11.8	11.5	9.60	9.30	7.97	8.32	7.42	9.34	2.79	12.7	8.76	4.73	18.5	12.2	164	62.3
Sm	2.26	2.33	2.57	2.28	2.50	2.14	2.33	1.80	2.33	0.75	1.73	1.78	1.26	1.54	2.09	19.62	6.06
Eu	0.83	0.88	0.94	0.80	0.90	0.82	0.65	0.73	0.90	0.25	0.70	0.53	0.41	0.49	0.58	3.49	1.23
Gd	2.81	2.81	2.98	2.72	2.79	2.23	2.33	2.40	3.07	1.42	2.20	2.22	1.70	1.41	2.80	9.58	3.39
Dy	3.10	3.20	2.86	2.84	2.95	3.47	3.64	3.14	3.36	2.01	2.97	2.68	2.42	2.05	3.01	5.36	3.26
Er	1.81	1.94	1.62	1.64	1.86	2.18	1.92	1.76	1.95	1.33	1.20	1.74	1.79	1.36	1.64	3.46	2.27
Yb	1.79	2.12	1.57	1.63	1.90	1.73	1.85	1.84	1.89	1.51	3.11	1.84	1.93	1.72	2.35	3.91	2.58
Pb	0.63	1.19	0.78	0.78	0.44	1.32	1.36	1.18	0.69	1.37	5.13	0.42	0.73	1.83	6.80	0.84	4.16
Th	0.66	1.28	1.15	0.83	0.29	9.95	8.98	2.98	0.77	5.37	3.88	9.00	2.11	2.31	2.05	6.65	2.89
U	0.19	0.33	0.30	0.24	0.09	3.04	3.15	0.69	0.24	2.14	2.01	3.10	0.70	0.69	0.92	1.60	0.70

1 pillow-rim glass D11-177, *2–9* ''normal'', group-I melt inclusions in high-Ca olivine, *6–8* high-K compositions within group-I, *10–17* ''anomalous'', group-II melt inclusions in low-Ca olivine, *16, 17* phosphorus-rich compositions within group-II. *Fo_Ol* mol% forsterite in host olivine, *CaO_Ol* wt% CaO content in host olivine. Photos of some analysed glass inclusions can be found on Fig. 1a (# 9, 10: m465a-18/1 and m465a-18/1), Fig. 1b (# 15, 16: m465b-7/1 and m465b-7/2), Fig. 9a (# 17: m465b-6/1) and Fig. 9c (# 12: m465a-2/1). Note compositional variations between some coexisting inclusions (e.g. # 9 and 10; # 15 and 16)

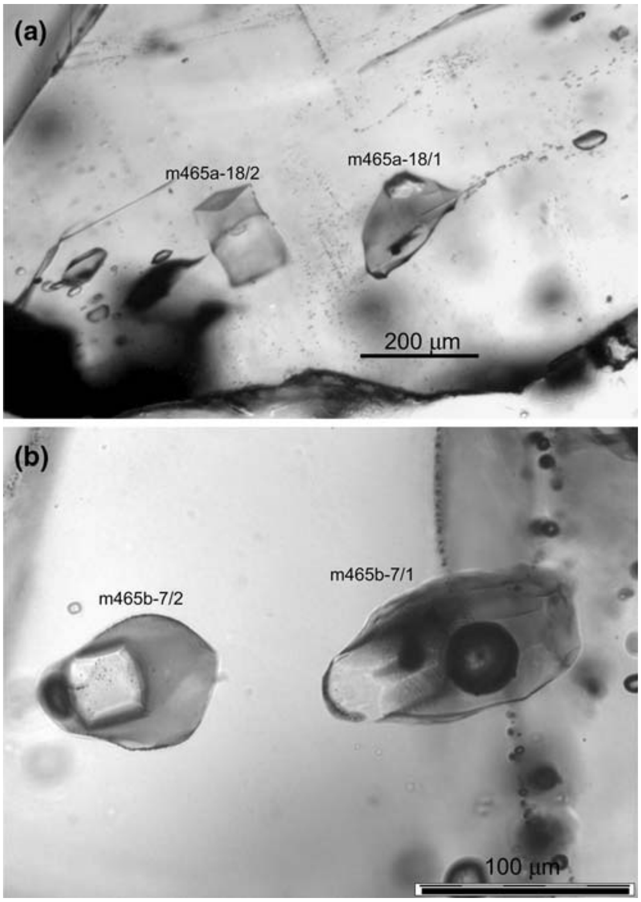

Fig. 1 Photos showing trails of olivine-hosted glass and vapour inclusions and coexistence of ''normal'' and ''anomalous'' melt inclusions (**a**) and ''anomalous'' melt inclusions with different composition and co-trapped orthopyroxene (**b**) within same olivine grains

Element mapping was performed to examine two-dimensional distribution of elements across sample surface. Measurements were done in the stage-scanning mode registering simultaneously X-ray signals of five wavelength dispersive spectrometers and back-scattered electron (BSE) image. Olivine was analysed for Mg, Al, Ca, Fe and Ni using TAP spectrometers for Mg and Al, PETJ for Ca, LIF for Fe and LIFH for Ni applying 20 kV accelerating voltage and 20 nA primary electron beam current. Step interval was 2 µm and X-ray acquisition time per step was 300 ms. Final evaluation of the measurement results were performed using the built-in JEOL Map Analysis Software.

Laser ablation ICP-MS

Trace element concentrations in melt inclusions were measured by laser ablation inductively coupled plasma mass spectrometry (LA-ICPMS) using a New Wave Research UP213 Nd-YAG (213 nm) laser coupled to an Agilent 4500 quadrupole mass-spectrometer (University of Tasmania, Australia). Analyses were performed in a He atmosphere by ablating 30–80 µm-diameter spots at a rate of 5 shots/s using laser power of ~12 J/cm^2. The instrument was optimized for sensitivity on mid- to high-mass isotopes (in the range 80–240 a.m.u.) and for minimal molecular oxide species (i.e., ^{232}Th^{16}O/^{232}Th < 0.2%) and doubly-charges ion species (i.e., $^{14°}$Ce^{++}/$^{14°}$Ce^{+} < 0.3%) production. The low level of molecular oxide and doubly charged ion production precludes the need to correct any of the analyte signal intensities for interfering species. The analysis time for each sample was 50–90 s, comprising a 30 s measurement of background (laser off) and a 20–60 s analysis (depending on inclusion's thickness) with laser on. Instrument calibration was performed by ablating the NIST612 glass standard. Data reduction was undertaken according to standard methods (Longerich et al. 1996) using the NIST612 glass as a primary reference material and ^{43}Ca (Ca analysed by EMPA) as the internal standard. USGS BCR-2g glass was repeatedly analysed throughout analytical sessions and was used as a secondary reference material.

Olivine and olivine-hosted inclusions

Olivine

Olivine phenocrysts analysed around inclusions of melt and spinel have limited compositional variations in terms of Fo content (89.8–91.1 mol%). Such compositions are very primitive among MORB olivine, which is typically < 89 mol% Fo, and rarely as high as 92 mol% Fo. Variations in CaO content are significant (0.15–0.35 wt%), and extend far below (i.e., <0.25 wt%) the values in primitive MORB olivine (Fig. 2). On the base of CaO abundances olivine crystals belong to two populations: dominant ''normal'' high-Ca (0.28–0.35 wt% CaO) and less abundant ''anomalous'' low-Ca (0.15–0.23 wt% CaO), with only three compositions in between (~0.25 wt% CaO). The first population, though overlapping with second population of olivine, is distinctively more magnesian (Fo90.1-91.1) than the second (Fo89.8-90.4). Single correlation trends of other analysed trace elements (positive for Al, Ni, Cr, and negative for Mn) with Fo do not allow discrimination between these two olivine populations (Fig. 2).

Distribution of major and trace elements within a single olivine crystal is studied using grain m465a-19

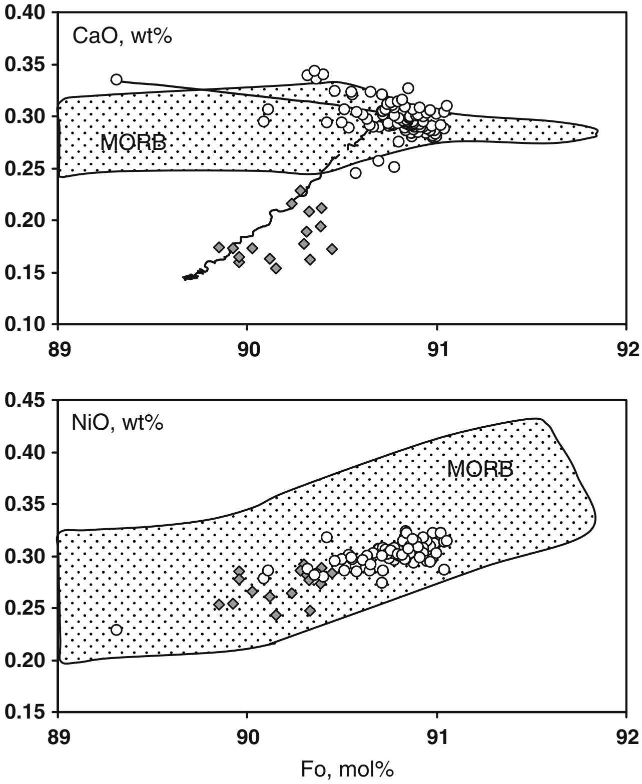

Fig. 2 Compositions of olivine phenocrysts (Fo vs. CaO, NiO): high-Ca "normal" olivine (*circles*); low-Ca, "anomalous" olivine (*diamonds*). The line shows changing olivine composition in zoned phenocryst m465a-19 (see Fig. 3 and text for more details). Compositional fields of MORB primitive olivine are shown

with clear compositional zoning in back-scattered electrons and sub-parallel trails of glass, vapour and sulphide inclusions (Fig. 3). Olivine outermost rim (~ 40 μm) shows extreme compositional zoning with Fo rapidly decreasing from 90.7 to 89.3 mol% towards the adjacent matrix glass, whereas MnO and CaO increase (0.16–0.19 wt% and 0.30–0.34 wt%, respectively) and NiO decrease (0.31–0.25 wt%). The rim has the most evolved Fo composition recorded in phenocrysts, but it is still more primitive than a hypothetical olivine in equilibrium with the matrix glass (Fo87.7, calculated with PETROLOG software (Danyushevsky 2001) and melt $Fe^{2+}/Fe^{3+} = 10$, as defined by matrix spinel compositions, Table 2). From the outermost rim this olivine fragment becomes gradually Fo- and CaO-poorer (90.7–89.8 mol% and 0.30–0.15 wt%, respectively, Fig. 3c,d) towards the core in which subparallel trails of melt and fluid inclusions are present (Fig. 3a). The core olivine (~300 μm of the profile) is fairly constant in composition (89.7 mol% Fo, 0.15 wt% CaO). Other trace elements change sympathetically with Fo along the profile (Fig. 3f–h). In general, compositional variations in this single olivine cover a significant part of the compositional range recorded for other olivine grains in the sample (Fig. 2).

Spinel inclusions

Most spinels are reddish-brown in colour and compositionally similar to spinel microphenocrysts in matrix glass and MORB spinel, in general (Allan et al. 1988; Kamenetsky et al. 2001a). They have relatively low TiO_2 (0.39–0.57 wt%) and moderately high Cr/(Cr + Al) (Cr# 0.53–0.62 mol%). These spinel grains are invariably hosted by "normal" high-Ca olivine (Fig. 4a; Table 2). In contrast, rare greenish-brown spinel inclusions are trapped in "anomalous" low-Ca olivine. These spinels are also unusual in composition in having extremely high TiO_2 (1.7–4.7 wt%) for spinel in primitive MORB (Allan et al. 1988; Kamenetsky and Crawford 1998; Kamenetsky et al. 2001a). They are also characterised by lower Cr_2O_3 abundances (35–42 wt%) than "normal" spinels (42–48 wt%) in this sample (Fig. 4b), but similar in terms of other elements. Importantly, the concentrations of "anomalous" elements, TiO_2 in greenish-brown spinel inclusions and CaO in host olivine, are negatively correlated (Fig. 4a). Two spinel inclusions exposed at surface of zoned olivine m465a-19 within 160 μm from each other (Fig. 3) have distinctively different TiO_2 (0.51 and 1.66 wt%), but similar other elements, and are hosted by olivine with 0.30 and 0.26 wt% CaO, respectively (Table 2).

Glass inclusions

All analysed glass inclusions are not in equilibrium with host olivine, because the trapped melts experienced depletion in MgO after olivine crystallisation on inclusions' walls and related "Fe-loss", as described by Danyushevsky et al. (2000). Thus, the inclusions have highly variable and positively correlated MgO and FeO contents (2.4–8.9 and 4.9–8.0 wt%, respectively, Table 1) that are lower than those in the pillow-rim glass and, by inference, in the originally trapped melts. In this particular case, corrections for post-trapped modifications are hampered by the fact that the original FeO content of some inclusions (see below) cannot be confidently inferred. However, we emphasize that post-entrapment modifications are not responsible for extreme variations in abundances of other major and trace elements observed in 93 analysed inclusions (Figs. 5, 6, 7, 8).

We use CaO content in the host olivine and CaO/Al_2O_3 ratio of the melt to primarily discriminate

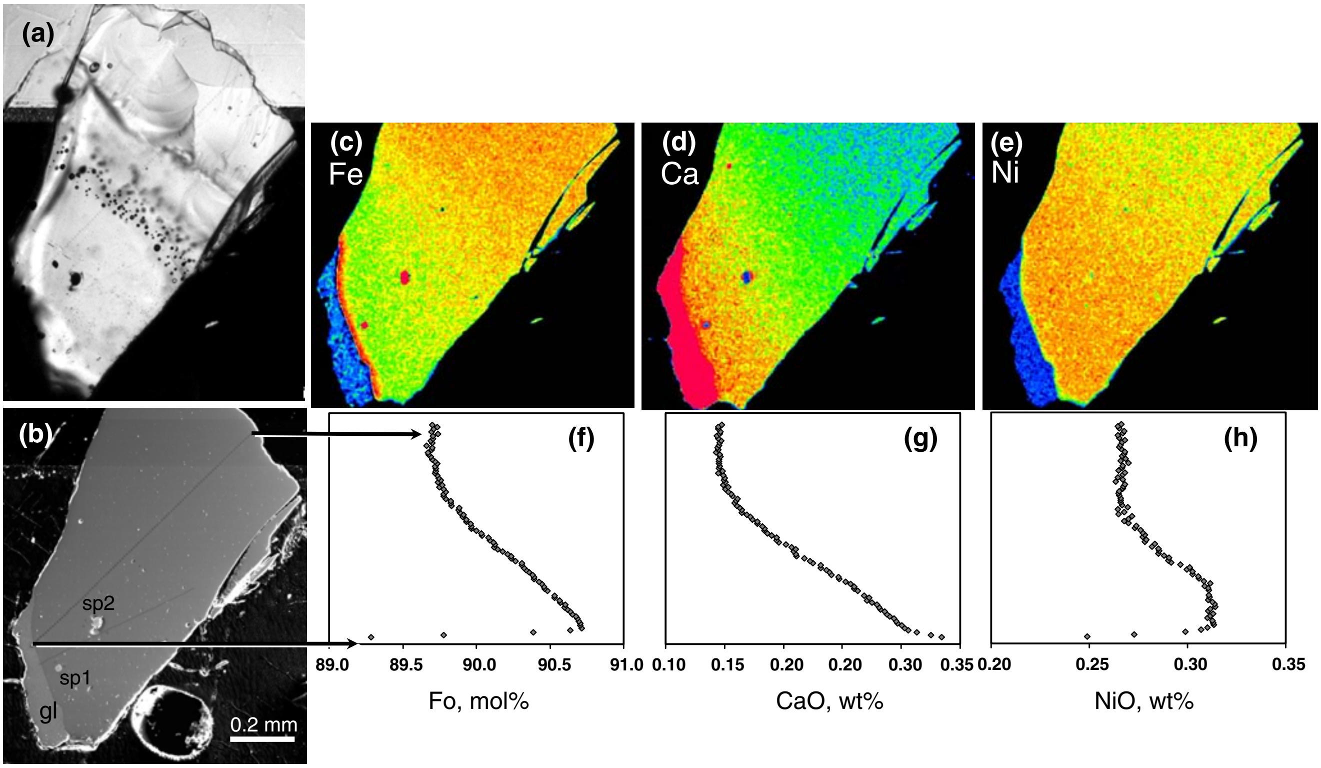

Fig. 3 Compositional zoning in a single olivine grain m465a-19: **a** optical image; **b** image in backscattered electrons showing glass, rimming the grain; two Cr- spinel inclusions (Table 2, # 4, 5) and two profile lines; **c–e** X-ray element maps showing distribution of Fe, Ca and Ni; **f–h** variations of Fo, CaO and NiO along the line shown on (**b**). Note the trails of melt, vapour and sulphide inclusions on (**a**) in low-Ca core part of this crystal

between compositions of trapped inclusions. The inclusions in the ''normal'' high-Ca olivine (hereafter, group-I) have high CaO/Al_2O_3 (0.91 ± 0.04) that broadly correlate with CaO in olivine (Fig. 6) and CaO/Al_2O_3 in the pillow-rim glass (0.87). In contrast, the inclusions in ''anomalous'' low-Ca olivine (hereafter, group-II), except three compositions, have significantly lower CaO/Al_2O_3 (0.54–0.67). Major compositional differences between two groups are outlined below.

Compositional trends shown by the group-I melt inclusions are largely controlled by post-entrapment crystallisation of olivine on the walls (e.g., trends for SiO_2, CaO and Al_2O_3; Fig. 5, Table 1). Importantly, the least affected by olivine crystallisation melt inclusions (with highest MgO) are compositionally similar to the pillow-rim glass (Fig. 5). The abundances of highly incompatible elements are strongly variable (e.g., 0.05–0.59 wt% K_2O, excluding four unusually K- and Cl-rich inclusions in this group), but on average they resemble the pillow-rim glass (cf. 0.33 ± 0.09 and 0.25 wt% K_2O, Figs. 5, 7a, 8). This is also typical of MORB magmatic process, in which variably enriched and depleted melt fractions aggregate in the plumbing system (Sobolev 1996; Shimizu 1998). The exceptions mentioned above, in addition to high K_2O (0.65–1.74 wt%) and Cl (0.15–0.20 wt%), demonstrated strongly elevated abundances of Rb, Th, U, Nb, Pb and Zr compared to other group-I inclusions and pillow-rim glass, and pronounced negative anomalies of Ba and Sr and positive Zr anomaly (Figs. 7c, 8; Table 1).

The compositions of group-II melt inclusions (Fig. 5; Table 1) are characteristically enriched in SiO_2 (52.9–58.5 wt%), TiO_2 (1.3–3.2) and Cl (0.04–0.25 wt%), but depleted in CaO (8.4–11.1 wt%) and S (0–0.08 wt%). The statistically lower FeO contents (4.9–6.7 wt%) in these inclusions, compared to group-I compositions (Fig. 5), suggest lower Fe abundances in the originally trapped melt, if the same extents of post-entrapment modifications of inclusions in both groups are assumed. Without a few exceptions the group-II inclusions also have lower Al_2O_3 and much higher Na_2O and K_2O than ''normal'' compositions in this study (Fig. 5). Strongly elevated abundances of TiO_2, K_2O and Cl are supplemented by the enrichment in the trace elements (Rb, Ba, Th, U, Pb, Sr and Zr), relative to rare-earth elements (REE) of similar incompatibility (by a factor of 3–8, Figs. 7b, 8). Notably, group-II inclusions

Table 2 Representative compositions of spinel inclusions in olivine phenocrysts and pillow-rim glass

N	1	2	3	4	5	6	7	8
Grain		m284-15/1	m465a-5/1	m465a-19/1	m465a-19/2	m284-32/1	m465b-8/1	m465a-15/1
SiO_2	0.35	0.47	0.08	0.10	0.09	0.37	0.15	0.15
TiO_2	0.43	0.39	0.57	0.51	1.66	2.46	2.81	4.68
Al_2O_3	22.73	25.19	21.45	24.19	23.33	22.13	22.95	22.62
Cr_2O_3	45.30	42.23	44.84	42.92	41.65	41.63	38.86	34.79
Fe_2O_3	3.89	4.06	4.82	4.94	4.91	4.41	5.20	5.95
FeO	11.15	10.57	11.21	10.48	11.35	12.66	12.12	13.32
MnO	0.18	0.18	0.09	0.08	0.08	0.18	0.19	0.07
MgO	16.40	17.07	15.87	16.84	16.79	16.53	16.69	16.95
NiO	0.17	0.19	0.16	0.18	0.20	0.20	0.21	0.24
Total	100.60	100.35	99.09	100.24	100.06	100.57	99.18	98.77
Mg#sp	72.4	74.2	71.6	74.1	72.5	69.9	71.1	69.4
Cr#sp	57.2	52.9	58.4	54.3	54.5	55.8	53.2	50.8
Fe^{2+}/Fe^{3+}	3.19	2.90	2.59	2.36	2.57	3.19	2.59	2.49
Host olivine								
SiO_2		40.69	40.67	40.45	40.55	40.98	40.44	40.61
FeO		8.82	9.44	8.90	9.09	9.42	9.46	9.79
MnO		0.14	0.16	0.14	0.15	0.16	0.16	0.16
MgO		49.90	49.37	49.53	49.64	49.71	49.55	49.17
CaO		0.28	0.34	0.30	0.26	0.21	0.21	0.16
NiO		0.32	0.29	0.30	0.31	0.29	0.28	0.28
Cr_2O_3		0.09	0.07	0.12	0.09	0.15	0.06	0.07
Total		100.24	100.34	99.74	100.09	100.92	100.16	100.24
Fo		91.0	90.3	90.8	90.7	90.4	90.3	90.0

1 average composition of spinel microphenocrysts ($n = 6$) in the pillow-rim glass, *2–4* "normal" spinel in high-Ca olivine, *5–8* "anomalous", high-Ti spinel trapped in low-Ca olivine. *Fo* mol% forsterite in olivine, *Mg#sp* spinel mg-number, 100 × Mg/(Mg + Fe^{2+}), atomic ratio, where Fe^{2+} and Fe^{3+} were calculated on the basis of spinel stoichiometry; *Cr#sp* spinel cr-number, 100 × Cr/(Cr + Al), atomic ratio. See Fig. 3 for location of spinel grains m465a-19/1 (#4) and m465a-19/2 (#5)

demonstrate progressive depletion in moderately incompatible REE (from Yb to Sm) relative to the pillow-rim glass, and increasing enrichment for more incompatible REE (from Nd to La) and Nb (Figs. 7b, 8). Such concave upward (U-shaped) REE pattern coupled with positive Zr anomaly resembles geochemical signature in boninites.

Three inclusions within the group-II can be considered the outliers in having elevated CaO/Al_2O_3 (078, 0.91 and 0.94), and distinctive other compositional features. The inclusion #m465b-1 has K_2O and P_2O_5 abundances <0.01 wt% and relatively low SiO_2 and Na_2O and high Al_2O_3 (Table 1). Two other inclusions, # m465b-6 and #m465b-7/2 (Fig. 1b), are the most enriched in P_2O_5 (1.2 and 4.6 wt%) and TiO_2 (2.6 and 4.9 wt%), but depleted in Al_2O_3 (14.4 and 13.4 wt%). In addition these inclusions are characterised by reduced SiO_2 (54.2 and 48.6 wt%) and elevated CaO (11.2 and 12.2 wt%) contents. The inclusion #m465b-7/2 (Fig. 1b) with the highest P_2O_5 and TiO_2 is the most enriched in REE, Nb, Sr and Zr, but shows strong relative depletions in Rb, K and Pb (Table 1).

Chemical variability of the inclusions in sample AII32 D11-177 is often pronounced on a very small spatial scale. Group-II inclusions in the grain #m465b-7, located within 60 μm from each other (Fig. 1b), are clearly different in terms of SiO_2, TiO_2, K_2O, P_2O_5 and Cl abundances (Table 1). Inclusions belonging to different compositional populations are found in close proximity (~150 μm) in grain m465a-18 (Fig. 1a; Table 1).

Orthopyroxene inclusions

Orthopyroxene crystals (15–50 μm) always associate with group-II glass in "anomalous" low-Ca olivine. Liquidus origin of orthopyroxene is suggested by euhedral shapes of orthopyroxene inclusions (Fig. 1b; 9) and swarms of tiny melt and fluid inclusions in some crystals (Figs. 1b, 9a). The large and variable size of orthopyroxene relative to the volume of associated glass (Figs. 1b, 9), with some cases of only a film of glass around orthopyroxene (Fig. 9d), argues for co-trapping, rather than post-entrapment crystallisation of the melt. Such chemical parameters as Mg/Fe (Mg# and Fo) and CaO contents are positively correlated in the orthopyroxene inclusions and their host olivine crystals (Table 3). The analysed orthopyroxene is compositionally unlike orthopyroxene from abyssal peridotites (Dick 1989; Elthon et al. 1992) in having much higher TiO_2 and lower Al_2O_3 and CaO (Table 3).

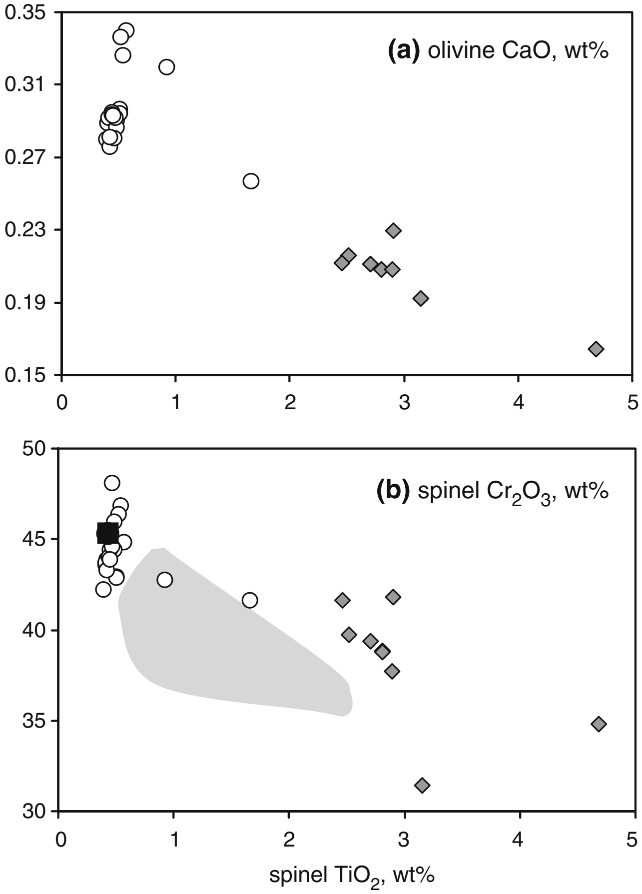

Fig. 4 Compositions of Cr-spinel inclusions trapped in high-Ca, "normal" olivine (*open circles*) and low-Ca, "anomalous" olivine (*diamonds*); and average composition of spinel microphenocrysts from the pillow-rim glass (*closed square*). Field shows spinel compositions for melt impregnated mantle and crustal rocks from Hess Deep and Garrett Transform fault (Hébert et al. 1983; Cannat et al. 1990; Hekinian et al. 1993; Allan and Dick 1996; Arai and Matsukage 1996; Dick and Natland 1996; Arai et al. 1997)

Discussion

Primary MORB magmas are compositionally variable owing to mantle heterogeneities, variations in melting degrees and pressure of melt segregation (Klein and Langmuir 1987; Kinzler and Grove 1992; Langmuir et al. 1992; Kamenetsky and Maas 2002; Niu et al. 2002). Additional changes to melt compositions, caused by reaction with lithospheric mantle and magmatic cumulates, are possibly superimposed on the original variability during magma ascent and residence in crustal magma chambers, respectively. Although efficient magma mixing within crustal magma chambers is believed to eliminate much of original and induced variability (Sobolev 1996), the erupted MORB magmas remain compositionally diverse on regional and local scale, but the degree of variability appears less than that ascribed to the melting processes (Kamenetsky et al. 2000; Kamenetsky and Maas 2002). However, primitive siliceous, orthopyroxene-bearing magmas, similar to the melt inclusions described above, have not been discovered to date among volcanic rocks and glasses at mid-oceanic ridges. The only known exception is the high-Mg andesitic glass bearing orthopyroxene microphenocrysts (S18-60/1) from the south Atlantic ridge near the Bouvet triple junction (Kamenetsky et al. 2001b), but the isotope composition of this glass (low $^{206}Pb/^{204}Pb = 17.188$ and $^{143}Nd/^{144}Nd = 0.511663$ and high $^{87}Sr/^{86}Sr = 0.712090$ and $\delta^{18}O = 6.8‰$), its high Ni (290 ppm) and strong "garnet signature" (Gd/Yb = 2.9) are not consistent with derivation from the oceanic upper mantle.

High-Si and orthopyroxene-bearing magmas among MORBs: peridotite melting scenarios

Oceanic cumulates can record MORB compositional diversity at the crystallisation stage, and thus allow tentative constraints on the composition of non-aggregated melts. From the study of gabbronorites with primitive orthopyroxene (Mg# up to 90 mol%) from the ODP Site 334, 104 km west of 37°N MAR, an unusually high SiO_2 (54 wt% at 10 wt% MgO) composition of the parental magmas was calculated by (Elthon et al. 1992). The SiO_2-rich melt parental to the Site 334 cumulates was also shown to be extremely depleted in Na_2O, TiO_2 and incompatible trace elements compared to any erupted MORB (Elthon et al. 1992; Ross and Elthon 1993). Consequently, the idea of SiO_2-rich basaltic liquids being "a widespread, but minor, component in mid-ocean ridge petrogenesis even though such liquids have never been directly sampled" (Elthon et al. 1992) and capable of crystallising orthopyroxene at low pressure was reconciled with the orthopyroxene-undersaturated nature of common primitive MORBs (O'Hara 1968; Stolper 1980).

Incidentally, at the time of the Site 334 cumulates study (Elthon et al. 1992; Ross and Elthon 1993), a high-SiO_2 (54.5 wt%) glass inclusion, ultradepleted in lithophile trace elements and associated with primitive orthopyroxene crystal (Mg# 90.8), was found in the olivine phenocryst from the basalt dredged between the Doldrums and Vema fracture zones on the Mid-Atlantic ridge, 9°N (Danyushevsky et al. 1987; Sobolev and Shimizu 1993b). Thus, the existence of the siliceous depleted magma in the mid-oceanic spreading environment, hypothesised in the study of gabbronorites (Elthon et al. 1992; Ross and Elthon 1993),

Fig. 5 Major element compositions of the pillow-rim glass (*square*) and melt inclusions trapped in high-Ca, ''normal'' olivine (group-I, *circles*) and low-Ca, ''anomalous'' olivine (group-II, *diamonds*). Four unusually K- and Cl-rich melt inclusions in group-I are represented by closed circles. Three melt inclusions, belonging to group-II but with elevated CaO/Al_2O_3 are shown by *open diamonds*

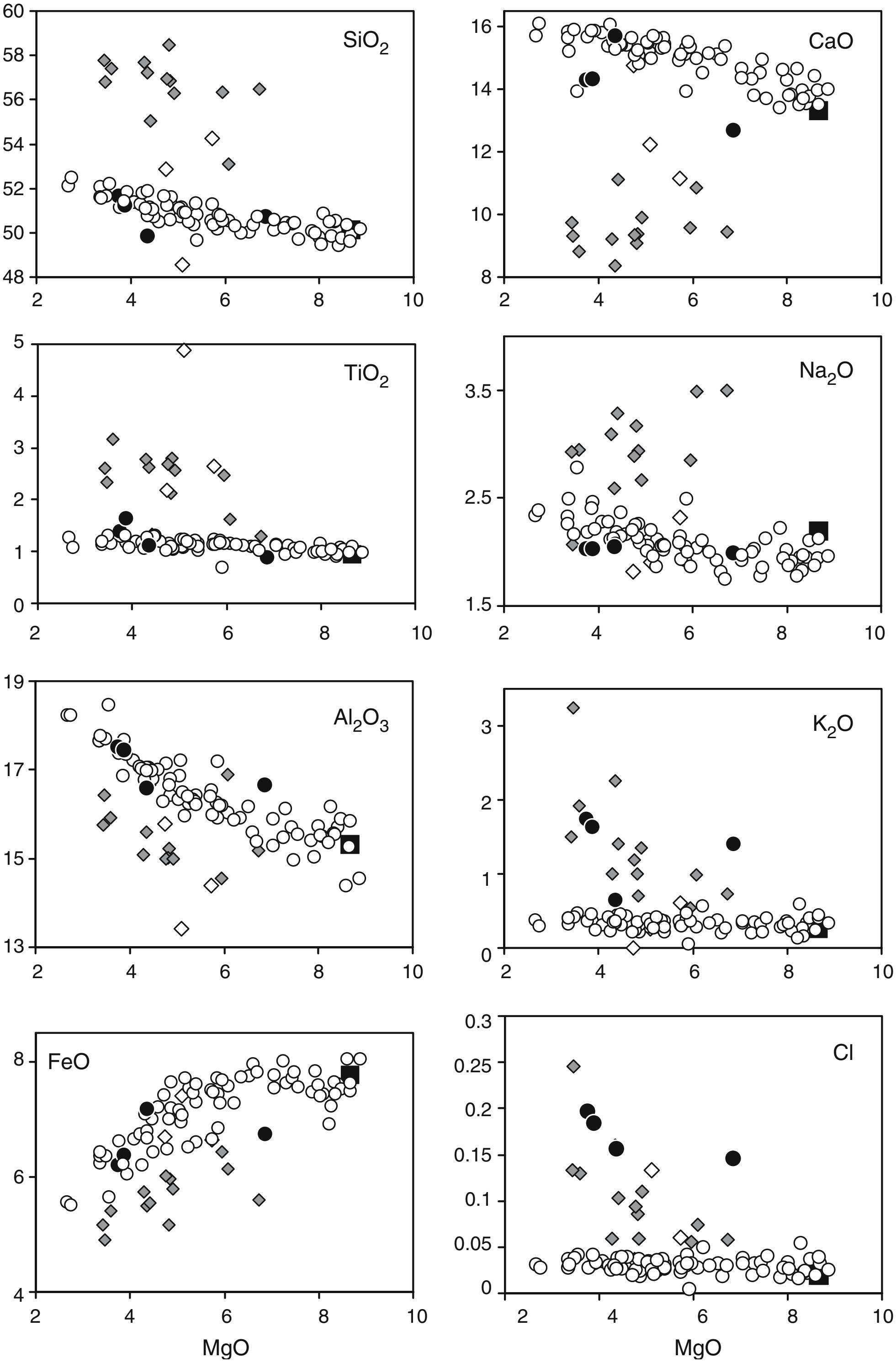

received direct support in the study of volcanic rocks (Danyushevsky et al. 1987; Sobolev and Shimizu 1993b). In both these studies the authors independently advocated the origin of high-SiO_2, orthopyroxene-saturated melt during shallow (2–5 kbar) critical (continuous) melting of already depleted mantle peridotite (clinopyroxene-poor harzburgite).

Recently a study of Sr isotope compositions of clinopyroxene in the DSDP Site 334 gabbronorites (Nonnotte et al. 2005) endorsed an alternative origin of

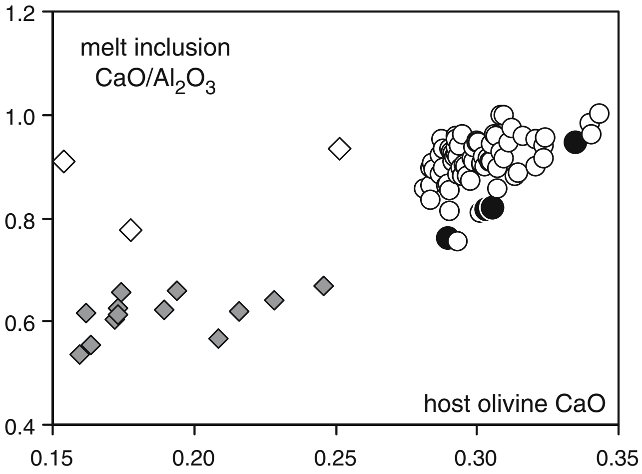

Fig. 6 Covariations between CaO/Al_2O_3 in melt inclusions and CaO content in host olivine phenocrysts. Symbols as in Fig. 5

parental melts for these unusual oceanic rocks. Based on evidence from the Oman ophiolite (Benoit et al. 1999), Nonnotte et al. (2005) proposed fluxing of very refractory mantle peridotites by hydrothermal fluids of crustal origin, followed by melting and formation of siliceous magmas with boninitic affinities.

High-Si and orthopyroxene-bearing magmas among MORBs: melt-peridotite reactions

Olivine gabbronorites and gabbronorites containing abundant primitive orthopyroxene (Mg# up to 88 mol%) were reported from the ODP Site 923 in the MARK area, south of the Kane fracture zone, 23°N MAR (Coogan et al. 2000a, b) and the ODP Sites 894–895 at Hess Deep, the East Pacific Rise (Hekinian et al. 1993; Arai and Matsukage 1996; Coogan et al. 2002). Saturation of magmas in ortho-

Fig. 7 Primitive mantle—normalised (Sun and McDonough 1989) trace element compositions of the melt inclusions in comparison to composition of the pillow-rim glass (*squares*)

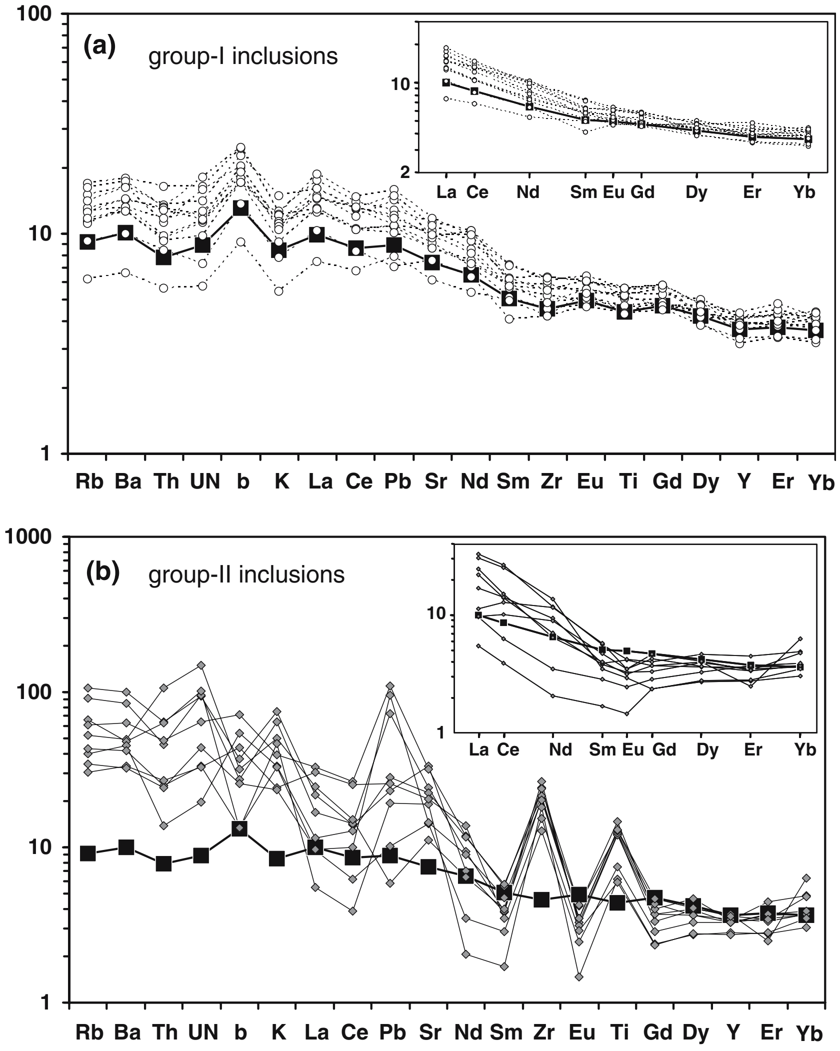

Fig. 7 continued

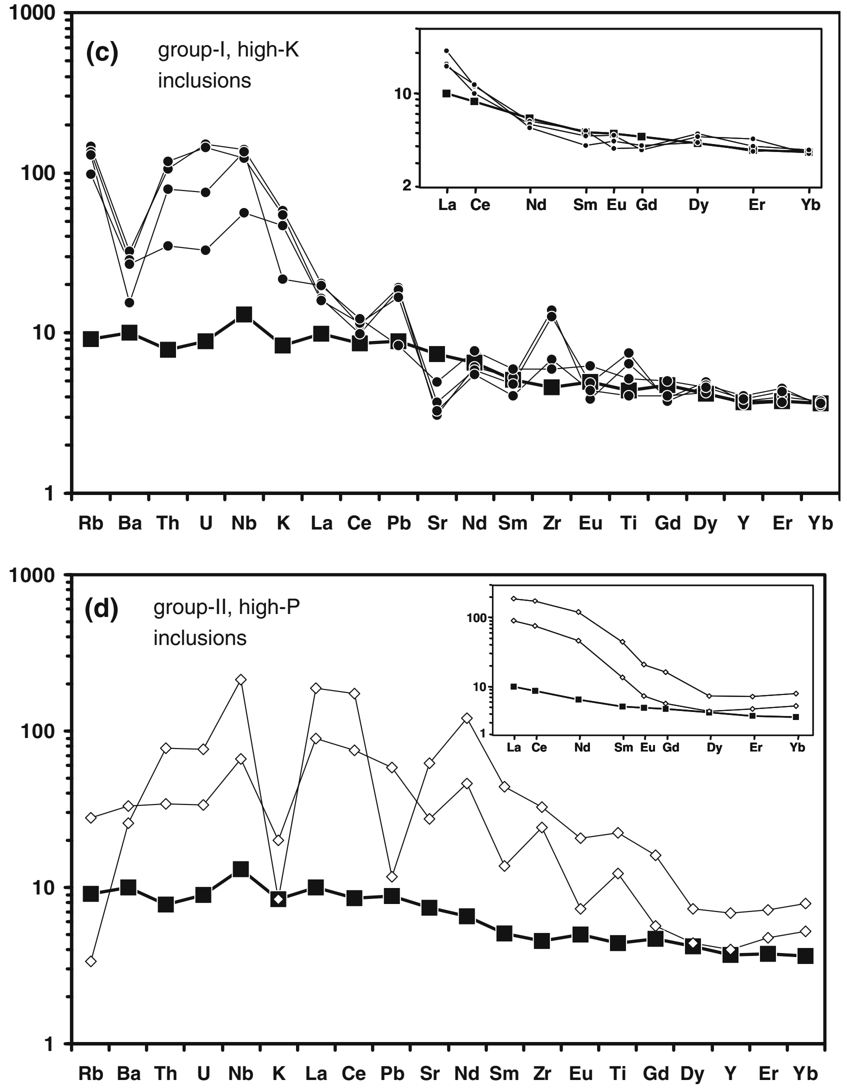

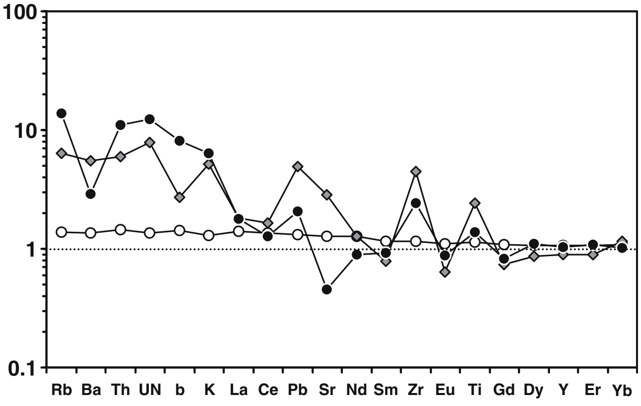

Fig. 8 Average trace element composition of melt inclusions (*circles* group-I, *closed circles* K- and Cl-enriched group-I; *diamonds* group-II), normalised to the composition of the pillow-rim glass AII32 D11-177

pyroxene and crystallisation of orthopyroxene-bearing cumulates has been explained by dissolution–reprecipitation reactions occurring during melt percolation through a harzburgitic peridotite (Coogan et al. 2002). Similar ideas of interactions between MORB-like melts and harzburgitic peridotite at low pressure, resulting in precipitation of olivine and clinopyroxene and dissolution of orthopyroxene, have been advocated in the previous study of the sample D11-177, 43°N MAR (Kamenetsky and Crawford 1998). Although shallow melting, especially in the presence of water, and melt re-equilibration with harzburgitic peridotite are still viable mechanisms for producing orthopyroxene-saturated MORB liquids, alternative origin of the association of low-Ca olivine, siliceous melts and orthopyroxene by assimilation of oceanic crust is proposed below.

Table 3 Representative compositions of orthopyroxene inclusions in olivine phenocrysts

N	1	2	3	4	5
Grain	m465a-2	m465b-1	m465b-6	m465b-7/1	m465b-7/2
SiO_2	57.16	56.28	56.77	57.21	57.46
TiO_2	0.23	0.18	0.34	0.38	0.17
Al_2O_3	0.84	1.18	1.15	0.81	0.45
FeO	6.33	5.89	6.24	6.43	6.21
MnO	0.17	0.15	0.15	0.15	0.15
MgO	34.71	33.84	34.81	35.02	35.28
CaO	1.29	1.78	1.11	0.92	0.72
Na_2O	0.03	0.04	0.02	0.03	0.02
Cr_2O_3	0.27	0.39	0.38	0.17	0.11
Total	101.03	99.73	100.97	101.12	100.57
Mg#opx	90.7	91.1	90.9	90.7	91.0
Host olivine					
CaO	0.22	0.25	0.18	0.15	0.16
NiO	0.26	0.30	0.29	0.24	0.25
Fo	90.2	90.8	90.3	90.2	90.3

Fo mol% forsterite in olivine, *Mg#opx* 100 × Mg/(Mg + Fe_{tot}), atomic ratio, where Fe_{tot} is total iron as FeO. See Figs. 1b and 9 for photos of orthopyroxene inclusions. The compositions of associated glass can be found in Table 1

High-Si and orthopyroxene-bearing magmas at 43°N MAR: reactions with oceanic crust?

The dominant population of high-Ca olivine and associated spinel inclusions in the studied sample D11-177 are typical of MORB primitive liquidus assemblage, and the compositions of group-I melt inclusions resemble the composition of the pillow-rim glass in this sample. Thus, these compositions are considered to be a ‘‘normal’’ MORB endmember in the processes controlling the trends towards unusual compositions in this sample.

In order to constrain the origin of unusual assemblage of low-Ca olivine, high-Ti spinel, orthopyroxene and high-Si melt inclusions in D11-177, we firstly made comparisons with other orthopyroxene-saturated melts recorded in mid-oceanic environments, such as the olivine-hosted melt inclusion from 9°N MAR (Sobolev and Shimizu 1993b) and parental magmas for the Site 334 cumulates (Elthon et al. 1992; Ross and Elthon 1993). Most striking differences are in that the group-II melt inclusions in this study are not depleted in incompatible trace elements as the previous records of high-Si magmas, but on contrary show strong enrich-

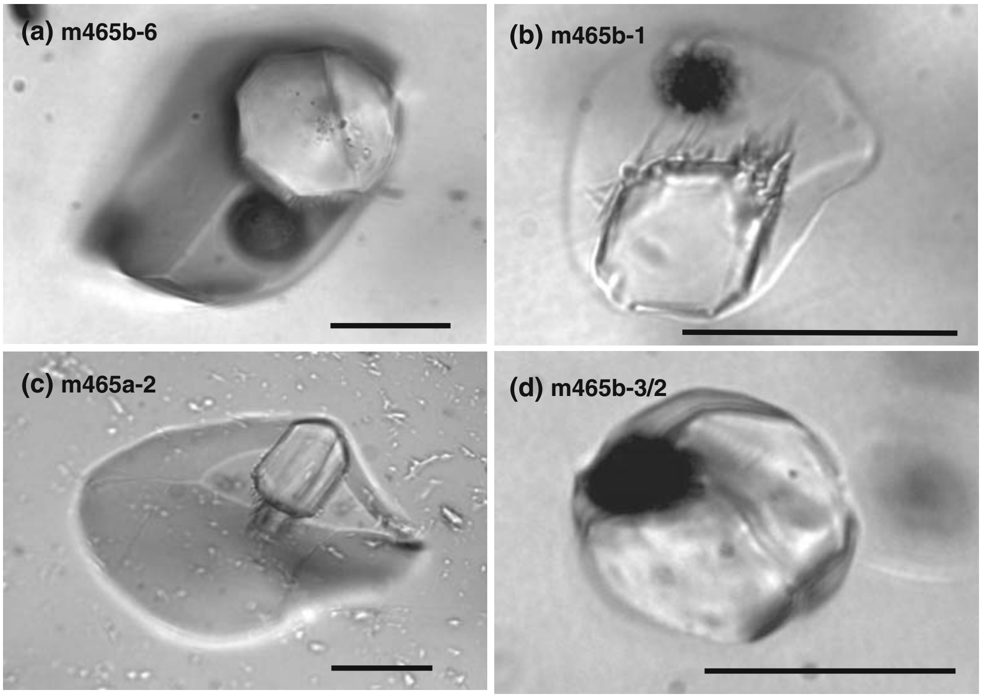

Fig. 9 Photos of orthopyroxene crystals coexisting with group-II melt (*glass*) in low-Ca, ‘‘anomalous’’ olivine. *Scale bars* are 30 μm

ment in these elements, as well as K_2O, Na_2O and TiO_2 (Figs. 5, 7, 8; Table 1). Orthopyroxene and spinel crystals in D11-177 are notably more TiO_2-rich (0.17–0.38 and 1–5 wt%, respectively) than "anomalous" orthopyroxene and spinel inclusions from 9°N MAR (0.04 and 0.17 wt%, respectively; Sobolev and Shimizu 1993b). Thus, decompressional melting of refractory peridotites at low pressure (Elthon et al. 1992; Sobolev and Shimizu 1993b) is unlikely mechanism to explain D11-177 melt and mineral compositions.

On the other hand, compositions of orthopyroxene and spinel from our study (Tables 2, 3) resemble primitive orthopyroxene (0.13–0.16 wt% TiO_2, 0.93–1.08 wt% Al_2O_3, 0.53–0.71 wt% CaO; Coogan et al. 2002) and high-Ti spinel in melt-impregnated crustal and mantle rocks from Hess Deep and Garrett Transform fault (Fig. 4b). Strong enrichment of the D11-177 spinel in TiO_2 relative to that of normal MORB (Fig. 4) requires unusual enrichment of parental melts in TiO_2 (2–5 wt%; Kamenetsky et al. 2001a), and this is in a good agreement with the observed TiO_2 abundances in the group-II melt inclusions (Fig. 5). Increasing abundances of TiO_2 in Cr-spinel are coupled with decreasing CaO in associated olivine (Fig. 4a), and are thus linked to decreasing CaO/Al_2O_3 (Fig. 6) and increasing SiO_2 in the melt inclusions. Importantly, in the trace element enriched group-II melt inclusions, TiO_2 (and Zr) demonstrate much stronger enrichment than the elements of similar incompatibility (Fig. 7b). Such preferential enrichment cannot be attributed to melt-peridotite reactions, as it requires a fractionation, induced by a Ti- and Zr-bearing mineral(s) (e.g., Ti-magnetite, ilmenite, rutile, zircon). Similarly, an apatite component is strongly pronounced in the composition of P-, Ca- and REE-enriched melt inclusions with relative depletion in K_2O, Rb and Pb (Fig. 7d). It also seems likely that other mineral phases, such as phlogopite and amphibole, can variably contribute to the "chaotic" geochemical patterns of the group-II (Fig. 7b) and group-I, high-K (Fig. 7c) melt inclusions. At the same time, the "anomalous" melt inclusions represent primitive (in terms of high Mg/Fe^{2+}) magmas, as their host olivine phenocrysts (>90 mol% Fo, Fig. 2, Table 1) are among most primitive olivine in MORB. The fact that in some "anomalous" inclusions certain elements fractionate from each other, whereas in other "anomalous" inclusions same elements covariate, suggests that extreme compositional variability among the "anomalous" inclusions in this study is a result of juxtaposition of melting/crystallisation processes in which minerals, atypical of primitive MORB assemblage, play important but differing roles. Where do these non-MORB minerals come into the processes contaminating compositions of primitive MORB magmas?

We, therefore, believe that the only source of mineralogical control on the melt anomalies in Ti, Zr, P and other trace elements, available beneath oceanic ridges, can be the lower plutonic oceanic crust (layer 3). This is dominantly composed of gabbroic cumulates, in which Ti-magnetite, ilmenite, zircon, amphibole and apatite are commonly recorded as late-magmatic or metasomatic accessory minerals (e.g., Hébert et al. 1991; Natland et al. 1991; Gillis and Meyer 2001; Meurer and Natland 2001; Natland and Dick 2001; Gillis et al. 2003; Sharkov et al. 2004, 2005; Koepke et al. 2005a). These minerals are suggested to be the first dissolving phases if their host gabbros are either fluxed with melts or fluids or heated above the solidus temperature. Strong involvement of apatite into the first melt pools and formation of immiscible P-enriched melts is argued by Koepke et al. (2005a), based on melting experiments with low-P_2O_5 (0.01 wt%) oceanic gabbros (Koepke et al. 2004, 2005b). It has been also suggested that local buffering by Fe-Ti oxides in the dissolution/precipitation reactions within oceanic cumulates can explain high TiO_2 content (2.2–4.4 wt%) of newly formed pargasitic amphibole, especially the grains containing relics of ilmenite (Koepke et al. 2005a). Similarly, assimilation of amphibole-oxide gabbros (ferrogabbros rich in Fe–Ti oxides) has been suggested to explain Ti-enriched compositions of Cr-spinel in the lowermost crust of the North Arm Mountain massif, Bay of Islands ophiolite (Bédard and Hébert 1998).

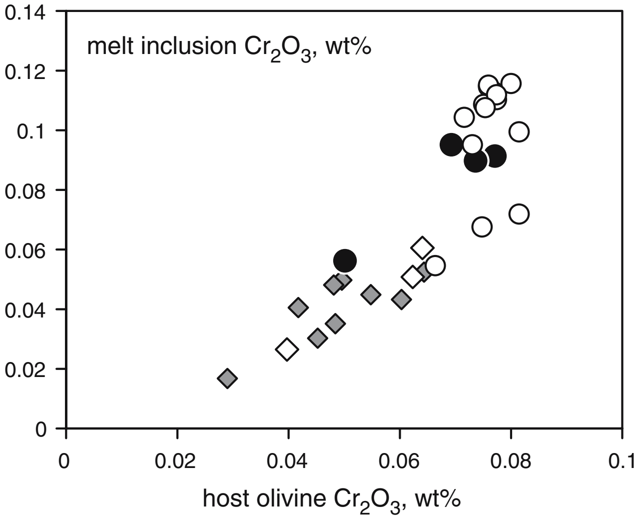

Fig. 10 Covariation of Cr_2O_3 in melt inclusions and their host olivine. *Symbols* as in Fig. 5

Contamination of MORB magmas with a component unusually enriched in SiO_2 and depleted in CaO (low CaO/Al_2O_3) is strongly pronounced in the majority of ''anomalous'' melt inclusions at 43°N MAR. The only major melt-mineral reaction that may cause the observed SiO_2 enrichment coupled with a pronounced decrease in CaO/Al_2O_3 is the incongruent melting of plagioclase, which would yield significant amounts of albite and orthoclase components into ''contaminated'' liquids. The presence of orthopyroxene crystals co-trapped with the high-Si melt inclusions (Figs. 1b, 9) suggests early magma saturation in this mineral. This is typical of boninites; moreover, U-shaped trace element patterns of these inclusions reinforce boninitic affinity (e.g., Crawford et al. 1989). However, relatively low Cr#, high-Ti compositions of spinel and ''dryness'' of melt inclusions (inferred from high microprobe totals, Table 1) are unlike those in boninites. Thus, depleted andesitic–boninitic magmas, derived from hydrated harzburgites at mid-ocean ridges (Nonnotte et al. 2005), are not considered here as a plausible contaminating component. Alternatively, the generation of silicic melts followed by precipitation of orthopyroxene, as recorded in hydrous partial melting experiments with natural oceanic gabbros at 900–1,060°C (Koepke et al. 2004, 2005b), represents in our case more realistic scenario for derivation of a high-Si melt contaminant from gabbro melting.

Scales of MORB melt contamination and diversity

Unlike well-established case of significant contamination of some MORB magmas by seawater-related Cl-rich components (e.g., Michael and Schilling 1989; Michael and Cornell 1998), the scale of contamination of primitive MORB by magmatic dissolution/precipitation reactions with crustal gabbroic cumulates or crystal mushes, as well as physical and chemical parameters of interacting melts, rocks and crystals, are not yet resolved quantitatively. The localised nature of the reaction processes and insignificant mixing between primitive MORB magmas and melts derived from crustal rocks and crystal mushes has been advocated by Danyushevsky et al. (2003, 2004) in the studies of melt inclusions from several MORB and subduction-related suites. Some trapped compositions were shown to record incongruent dissolution of individual plagioclase or clinopyroxene crystals (Danyushevsky et al. 2003, 2004). As discussed above, some ''anomalous'' melt inclusion compositions in our study were unambiguously contributed from distinct Ti-, P-, and K-bearing minerals, however, the general high-Si and low-Ca compositional signature of the contaminant requires melting of a multiphase assemblage (rock or/and crystal mush) at the interface with hot MORB magma (Bédard et al. 2000). A population of ''anomalous'' low-Ca olivine (see also Kamenetsky et al. 2006) crystallising in a contaminated boundary layer (CBL) and trapping ''anomalous'' inclusions of melt, orthopyroxene and Ti-rich spinel is a good evidence for ''incomplete mixing in these contaminated boundary layers'' (Bédard et al. 2000). Occurrence of ''anomalous'' melt inclusions of variable composition (Figs. 5, 7, 8), and in particular within a single olivine crystal in close proximity to each other (grain #m465b-7, Fig. 1b, Table 1, # 16, 17) further suggests that CBL is compositionally heterogeneous. Another interesting feature of the CBL magma is saturation in volatiles (presumably CO_2) and sulphide melt as evidenced by common occurrence of gaseous bubbles and sulphide globules in low-Ca olivine (Figs. 1, 3). The CBL must be also saturated with Cr-spinel (Fig. 10) that crystallises and accumulates in greater than cotectic proportions in this specific environment (Bédard and Hébert 1998).

If CBL is not particularly oxidised (see data on Fe^{2+}/Fe^{3+} in spinel, Table 2) its Mg# is only marginally lower than Mg# of the MORB melt in this case, as it follows from the olivine compositions (Fig. 2, Tables 1, 2, 3). The high Fo compositions of ''anomalous'' olivine at 43°N MAR are consistent with the conclusions of Danyushevsky et al. (2004) that ''anomalous'' inclusions are preferentially trapped in forsteritic olivine. On the other hand, the partial melts of gabbros at the temperature of primitive MORB magma are expected to be saturated with high-Fo olivine (Koepke et al. 2004), although the control from oxygen fugacity is not to be forgotten.

Do other contrasting chemical parameters tend to homogenise by either diffusion or mingling, so CBL undergoes destruction and MORB magmas are contaminated? The coexistence of ''normal'' and ''anomalous'' melt inclusions within a single olivine crystal (grain m465a-18, Fig. 1a, Table 1, # 9, 10) and gradual zoning in the olivine grain m465a-19 (from low-Ca core with high-Ti spinel towards ''normal'' rims with ''normal'' spinel; Fig. 3, Table 2, # 4 and #5) is a strong argument for that mixing between CBL and MORB melts indeed occurred. However, the degree of mixing at each particular stage of olivine crystallisation remains unknown, and thus quantitative constraints on a chemical identity of CBL (which is primarily heterogeneous; see above) and its ''contaminating'' effect on the mantle-derived MORB melt have no unique solution.

The contamination of primary melts forming MORB with CBL adds to original diversity generated in the processes of mantle melting. Similar to averaging primary MORB compositions, locally contaminated melts are prone to aggregation prior to eruption, and thus the effects of contamination can be effectively masked in the erupted magmas. It is worth noting that magma contamination by interaction with crustal rocks is complimented by chemical and mineralogical changes in these rocks (assimilation), and such changes are by far readily recognised than the magma contamination. Different mechanisms have been accounted for melting and recrystallisation in oceanic gabbroic cumulates, and among them assimilation of crustal cumulates by hot primitive MORB melts is not to be ignored in future studies.

Acknowledgments Discussions with Leonid Danyushevsky and Ilya Veksler triggered ‘‘crustal’’ explanations for mantle-derived samples. We thank an anonymous reviewer for helpful and constructive comments on the manuscript. Al Hofmann and Alex Sobolev provided access to instrumentation at the Max Planck Institute, Mainz. This work was supported by the A. von Humboldt Foundation (Friedrich Wilhelm Bessel Award to Vadim Kamenetsky and Wolfgang Paul Award to A.V. Sobolev), the Max Planck Society and Australian Professorial Fellowship and Discovery Grant to VSK.

References

Allan JF, Dick HJB (1996) Cr-rich spinel as a tracer for melt migration and melt-wall rock interaction in the mantle: Hess Deep, Leg 147. In: Mevel C, Gillis KM, Allan JF, Meyer PS (eds) Proceedings of ODP, Sci results, vol 147, College Station, pp 157–172

Allan JF, Sack RO, Batiza R (1988) Cr-rich spinels as petrogenetic indicators: MORB-type lavas from the Lamont seamount chain, eastern Pacific. Am Mineral 73:741–753

Amri I, Benoit M, Ceuleneer G (1996) Tectonic setting for the genesis of oceanic plagiogranites: evidence from a paleo-spreading structure in the Oman ophiolite. Earth Planet Sci Lett 139:177–194

Arai S, Matsukage K (1996) Petrology of gabbro-troctolite-peridotite complex from Hess Deep, equatorial Pacific: implications for mantle-melt interaction within the oceanic lithosphere. In: Mevel C, Gillis KM, Allan JF, Meyer PS (eds) Proceedings of ODP, Sci results, vol 147, College Station, pp 135–155

Arai S, Matsukage K, Isobe E, Vysotskiy S (1997) Concentration of incompatible elements in oceanic mantle: effect of melt/wall interaction in stagnant or failed melt conduits within peridotite. Geochim Cosmochim Acta 61:671–675

Bédard JH (1991) Cumulate recycling and crustal evolution in the Bay of Islands Ophiolite. J Geol 99:225–249

Bédard JH (1993) Oceanic crust as a reactive filter: Synkinematic intrusion, hybridization, and assimilation in an ophiolitic magma chamber, western Newfoundland. Geology 21:77–80

Bédard JH, Hébert R (1996) The lower crust of the Bay of Islands ophiolite, Canada: petrology, mineralogy, and the importance of syntexis in magmatic differentiation in ophiolites and at ocean ridges. J Geophys Res 101:25105–25124

Bédard JH, Hébert R (1998) Formation of chromitites by assimilation of crustal pyroxenites and gabbros into peridotitic intrusions—North Arm Mountain Massif, Bay of Islands Ophiolite, Newfoundland, Canada. J Geophys Res 103:5165–5184

Bédard JH, Hébert R, Berclaz A, Varfalvy V (2000) Syntexis and the genesis of lower oceanic crust. In: Dilek Y, Moores EM, Elthon D, Nicolas A (eds) Ophiolites and oceanic crust: new insights from field studies and the ocean drilling program, spec paper 349. Geological Society of America, Boulder, Colorado, pp 105–119

Benoit M, Ceuleneer G, Polve M (1999) The remelting of hydrothermally altered peridotite at mid-ocean ridges by intruding mantle diapirs. Nature 402:514–518

Cannat M, Bideau D, Hébert R (1990) Plastic deformation and magmatic impregnation in serpentinized ultramafic rocks from the Garrett transform fault (East Pacific Rise). Earth Planet Sci Lett 101:216–232

Coogan L, Saunders A, Kempton P, Norry M (2000a) Evidence from oceanic gabbros for porous melt migration within a crystal mush beneath the Mid-Atlantic Ridge. Geochem Geophys Geosyst 1, Paper number 2000GC000072

Coogan LA, Kempton PD, Saunders AD, Norry MJ (2000b) Melt aggregation within the crust beneath the Mid-Atlantic Ridge: evidence from plagioclase and clinopyroxene major and trace element compositions. Earth Planet Sci Lett 176:245–257

Coogan LA, Gillis KM, MacLeod CJ, Thompson GM, Hekinian R (2002) Petrology and geochemistry of the lower ocean crust formed at the East Pacific Rise and exposed at Hess Deep: A synthesis and new results. Geochem Geophys Geosyst 3. DOI 10.1029/2001GC000230

Crawford AJ, Falloon TJ, Green DH (1989) Classification, petrogenesis and tectonic setting of boninites. In: Crawford AJ (eds) Boninites. Unwin Hyman, London, pp 1–49

Danyushevsky LV (2001) The effect of small amounts of H2O on crystallisation of mid-ocean ridge and backarc basin magmas. J Volcanol Geotherm Res 110:265–280

Danyushevsky LV, Sobolev AV, Dmitriev LV (1987) Low-titanium orthopyroxene-bearing tholeiite, a new type of ocean-rift tholeiite. Trans (Doklady) USSR Acad Sci 292:102–105

Danyushevsky LV, Della-Pasqua FN, Sokolov S (2000) Re-equilibration of melt inclusions trapped by magnesian olivine phenocrysts from subduction-related magmas: petrological implications. Contrib Mineral Petrol 138:68–83

Danyushevsky LV, Perfit MR, Eggins SM, Falloon TJ (2003) Crustal origin for coupled ‘ultra-depleted’ and ‘plagioclase’ signatures in MORB olivine-hosted melt inclusions: evidence from the Siqueiros transform fault, East Pacific rise. Contrib Mineral Petrol 144:619–637

Danyushevsky LV, Leslie RAJ, Crawford AJ, Durance P (2004) Melt inclusions in primitive olivine phenocrysts: the role of localized reaction processes in the origin of anomalous compositions. J Petrol 45:2531–2553

Dick HJB (1989) Abyssal peridotites, very slow spreading ridges and ocean ridge magmatism. In: Sounders AD, Norry MJ (eds) Magmatism in the ocean basins, vol 42. Geol Soc Spec Publ, London, pp 71–105

Dick HJB, Natland JH (1996) Late-stage melt evolution and transport in the shallow mantle beneath the East Pacific Rise. In: Mevel C, Gillis KM, Allan JF, Meyer PS (eds) Proceedings of ODP, science results, vol 147, College Station, pp 103–134

Dixon JE, Clague DA, Stolper EM (1991) Degassing history of water, sulfur and carbon in submarine lavas from Kilauea volcano, Hawaii. J Geol 99:371–394

Elthon D, Stewart M, Ross DK (1992) Compositional trends of minerals in oceanic cumulates. J Geophys Res 97:15189–15199

Gillis K, Coogan L, Chaussidon M (2003) Volatile element (B, Cl, F) behaviour in the roof of an axial magma chamber from the East Pacific Rise. Earth Planet Sci Lett 213:447–462

Gillis KM, Meyer PS (2001) Metasomatism of oceanic gabbros by late stage melts and hydrothermal fluids: Evidence from the rare earth element composition of amphiboles. Geochem Geophys Geosyst 2, Art. No. 2000GC000087

Hébert R, Bideau D, Hekinian R (1983) Ultramafic and mafic rocks from the Garrett Transform Fault near 13°30′S on the East Pacific Rise: igneous petrology. Earth Planet Sci Lett 65:107–125

Hébert R, Constantin M, Robinson PT (1991) Primary mineralogy of Leg 118 gabbroic rocks and their place in the spectrum of oceanic mafic igneous rocks. In: Von Herzen RP, Robinson PT et al (eds) Proceedings of ODP, science results, vol 118, College Station, pp 3–19

Hekinian R, Bideau D, Francheteau J, Cheminee JL, Armijo R, Lonsdale P, Blum N (1993) Petrology of the East Pacific Rise crust and upper mantle exposed in Hess Deep (Eastern Equatorial Pacific). J Geophys Res 98:8069–8094

Hofmann AW (2003) Sampling mantle heterogeneity through oceanic basalts: Isotopes and trace elements. In: Holland H, Turekian KK (eds) Treatise on geochemistry. vol 2. Elsevier-Pergamon, Oxford, pp 61–101

Ito E, White WM, Gopel C (1987) The O, Sr, Nd and Pb isotope geochemistry of MORB. Chem Geol 62:157–176

Jarosewich EJ, Nelen JA, Norberg JA (1980) Reference samples for electron microprobe analysis. Geostandards Newslett 4:43–47

Kamenetsky V, Crawford AJ (1998) Melt-peridotite reaction recorded in the chemistry of spinel and melt inclusions in basalt from 43°N, Mid-Atlantic Ridge. Earth Planet Sci Lett 164:345–352

Kamenetsky VS, Maas R (2002) Mantle-melt evolution (dynamic source) in the origin of a single MORB suite: a perspective from magnesian glasses of Macquarie Island. J Petrol 43:1909–1922

Kamenetsky VS, Eggins SM, Crawford AJ, Green DH, Gasparon M, Falloon TJ (1998) Calcic melt inclusions in primitive olivine at 43°N MAR: Evidence for melt-rock reaction/melting involving clinopyroxene-rich lithologies during MORB generation. Earth Planet Sci Lett 160:115–132

Kamenetsky VS, Everard JL, Crawford AJ, Varne R, Eggins SM, Lanyon R (2000) Enriched end-member of primitive MORB melts: petrology and geochemistry of glasses from Macquarie Island (SW Pacific). J Petrol 41:411–430

Kamenetsky VS, Crawford AJ, Meffre S (2001a) Factors controlling chemistry of magmatic spinel: an empirical study of associated olivine, Cr-spinel and melt inclusions from primitive rocks. J Petrol 42:655–671

Kamenetsky VS, Maas R, Sushchevskaya NM, Norman M, Cartwright I, Peyve AA (2001b) Remnants of Gondwanan continental lithosphere in oceanic upper mantle: evidence from the South Atlantic Ridge. Geology 29:243–246

Kamenetsky VS, Elburg M, Arculus RJ, Thomas R (2006) Phenocrystic origin of low-Ca olivines in subduction-related magmas: implications for magma petrogenesis. Chem Geol 233:346–357

Kinzler RJ, Grove TL (1992) Primary magmas of mid-ocean ridge basalts 2. Applications. J Geophys Res 97:6907–6926

Klein EM, Langmuir CH (1987) Global correlations of ocean ridge basalt chemistry with axial depth and crustal thickness. J Geophys Res 92:8089–8115

Koepke J, Feig ST, Snow J, Freise M (2004) Petrogenesis of oceanic plagiogranites by partial melting of gabbros: an experimental study. Contrib Mineral Petrol 146:414–432

Koepke J, Feig S, Snow J (2005a) Late stage magmatic evolution of oceanic gabbros as a result of hydrous partial melting: Evidence from the Ocean Drilling Program (ODP) Leg 153 drilling at the Mid-Atlantic Ridge. Geochem Geophys Geosyst 6:Q02001. DOI 10.1029/2004GC000805

Koepke J, Feig ST, Snow J (2005b) Hydrous partial melting within the lower oceanic crust. Terra Nova 17:286–291

Langmuir CH, Klein EM, Plank T (1992) Petrological systematics of mid-ocean ridge basalts: constraints on melt generation beneath ocean ridges. In: Phipps Morgan J, Blackman DK, Sinton JM (eds) Mantle flow and melt generation at mid-ocean ridges, vol 71. Geophys Monogr Ser AGU, Washington, pp 183–280

Longerich HP, Jackson SE, Gunther D (1996) Laser ablation inductively coupled plasma mass spectrometric transient signal data acquisition and analyte concentration calculation. J Anal Atom Spectr 11:899–904

Métrich N, Bertagnini A, Landi P, Rosi M (2001) Crystallization driven by decompression and water loss at Stromboli volcano (Aeolian Islands, Italy). J Petrol 42:1471–1490

Meurer WP, Natland JH (2001) Apatite compositions from oceanic cumulates with implications for the evolution of mid-ocean ridge magmatic systems. J Volcanol Geotherm Res 110:281–298

Michael PJ, Cornell WC (1998) Influence of spreading rate and magma supply on crystallization and assimilation beneath mid-ocean ridges: evidence from chlorine and major element chemistry of mid-ocean ridge basalts. J Geophys Res 103:18325–18356

Michael P, Schilling J-G (1989) Chlorine in mid-ocean ridge magmas: evidence for assimilation of seawater-influenced components. Geochim Cosmochim Acta 53:3131–3143

Natland JH, Dick HJB (2001) Formation of the lower ocean crust and the crystallization of gabbroic cumulates at a very slowly spreading ridge. J Volcanol Geotherm Res 110:191–233

Natland JH, Meyer PS, Dick HJB, Bloomer SH (1991) Magmatic oxides and sulfides in gabbroic rocks from Hole 735B and the later development of the liquid line of descent. In: Von Herzen RP, Robinson PT et al (eds) Proceedings of ODP, science results, vol 118, College Station, pp 75–111

Niu Y, Regelous M, Wendt IJ, Batiza R, O'Hara MJ (2002) Geochemistry of near-EPR seamounts: importance of source vs. process and the origin of enriched mantle component. Earth Planet Sci Lett 199:327–345

Nonnotte P, Ceuleneer G, Benoit M (2005) Genesis of andesitic-boninitic magmas at mid-ocean ridges by melting of hydrated peridotites: geochemical evidence from DSDP Site 334 gabbronorites. Earth Planet Sci Lett 236:632–653

O'Hara MJ (1968) Are any ocean-floor basalts primary magmas? Nature 220:683–686

Phillips JD, Thopmson G, Von Herzen RP, Bowen VT (1969) Mid-Atlantic Ridge near 43°N latitude. J Geophys Res 74:3069–3081

Ross K, Elthon D (1993) Cumulates from strongly depleted mid-ocean-ridge basalt. Nature 365:826–829

Sharkov EV, Bortnikov NS, Bogatikov OA, Belyatskii BV, Zinger TF, Skolotnev SG (2004) Mesozoic zircon from gabbronorites of the axial Mid-Atlantic Ridge, 6° N, Markov Deep. Dokl. Earth Sci 397:654–657

Sharkov EV, Bortnikov NS, Bogatikov OA, Zinger TF, Bel'tenev VE, Chistyakov AV (2005) Third layer of the oceanic crust in the axial part of the Mid-Atlantic Ridge (Sierra Leone MAR segment, 6° N). Petrology 13:540–570

Shibata T, Thompson G (1986) Peridotites from the Mid-Atlantic Ridge at 43°N and their petrogenetic relation to abyssal tholeiites. Contrib Mineral Petrol 93:144–159

Shibata T, Thompson G, Frey FA (1979) Tholeiitic and alkali basalts from the Mid-Atlantic Ridge at 43°N. Contrib Mineral Petrol 70:127–141

Shimizu N (1998) The geochemistry of olivine-hosted melt inclusions in a FAMOUS basalt ALV519–4–1. Phys Earth Planet Inter 107:183–201

Sobolev AV (1996) Melt inclusions in minerals as a source of principle petrological information. Petrology 4:228–239

Sobolev AV, Shimizu N (1993a) Superdepleted melts and ocean mantle permeability. Trans (Doklady) Russ Acad Sci 328:182–188

Sobolev AV, Shimizu N (1993b) Ultra-depleted primary melt included in an olivine from the Mid-Atlantic Ridge. Nature 363:151–154

Stolper E (1980) A phase diagram for mid-ocean ridge basalts: preliminary results and implications for petrogenesis. Contrib Mineral Petrol 74:13–27

Sun S-S, McDonough WF (1989) Chemical and isotopic systematics of oceanic basalts: implications for mantle composition and processes. In: Saunders AD, Norry MJ (eds) Magmatism in the ocean basins, vol 42. Geol Soc Spec Publ, London, pp 313–345

Thordarson T, Self S, Oskarsson N, Hulsebosch T (1996) Sulfur, chlorine, and fluorine degassing and atmospheric loading by the 1783–1784 AD Laki (Skaftár Fires) eruption in Iceland. Bull Volcanol 58:205–225

Yu D, Fontignie D, Schilling JG (1997) Mantle plume-ridge interactions in the Central North Atlantic: a Nd isotope study of Mid-Atlantic Ridge basalts from 30°N to 50°N. Earth Plnet Sci Lett 146:259–272